https://doi.org/10.5194/egusphere-2025-5608
Preprint. Discussion started: 16 January 2026

SNOWstorm (v1.0) - a deep-learning based model for near-surface winds and drifting snow in mountain environments

Manuel Saigger[1], Brigitta Goger[2], and Thomas Mölg[1]

[1]Climate System Research Group, Institute of Geography, Friedrich-Alexander-Universität (FAU) Erlangen-Nürnberg, Erlangen, Germany
[2]Center for Climate Systems Modeling, ETH Zurich, Zurich, Switzerland, now at: GeoSphere Austria

Correspondence: Manuel Saigger (manuel.saigger@fau.de)

Abstract. Wind-driven redistribution of snow and resulting heterogeneous snow accumulation poses a major uncertainty in mountain hydrology and distributed glacier mass balance models as it is often neglected. High-quality information on the fine-scale wind structure is crucial to predict snow redistribution, but past approaches either relied on highly simplified assumptions or on computationally expensive numerical simulations, inhibiting the application for long-term studies.

To bridge this gap, we introduce SNOWstorm – the snow drift sublimation and transport model. It is designed as a deep-learning based emulator model, that is trained on data from high-resolution (Δx =50 m) numerical simulations in semi-idealized conditions, to be applicable over a wide range of atmospheric conditions and for a wide range of mountain regions. The model can be driven with input of standard atmospheric variables from coarse- to meso-scale numerical models and predicts near-surface wind fields, and rates of wind-driven snow mass change, drifting snow sublimation and snow transport. Validation experiments show that the model reproduces major terrain-induced flow features as well as patterns of snow redistribution. In a first real-world application study in the European Alps, SNOWstorm predicts wind fields and drifting snow patterns comparable to nested numerical large-eddy simulations, though at more than five orders of magnitude less computational expense. The model thus shows the potential to be used in future studies on multi-seasonal influence of snow redistribution on glacier mass balance in various climatic settings.

1 Introduction

Snow accumulation in mountain environments can strongly differ over short distances. This heterogeneous snow accumulation can play an essential role in mountain hydrology, glacier mass balance or avalanche risk. Therefore, a representation of this variability is crucial for reliable glacier projections, run-off forecasts, weather predictions and avalanche risk assessments. The underlying processes leading to the variability in snow accumulation are classically divided into pre- and post-depositional processes (Mott et al., 2018). Pre-depositional processes include orographic precipitation enhancement, cloud-microphysical and thermodynamic interactions of snow particles with the surrounding atmosphere, as well as interaction with near-surface flow features leading to preferential deposition of snowfall (e.g. Zängl, 2007; Houze, 2012; Mott et al., 2014; Vionnet et al., 2017; Gerber et al., 2019). Post-depositional redistribution mainly takes place due to avalanches and drifting and blowing snow.

https://doi.org/10.5194/egusphere-2025-5608
Preprint. Discussion started: 16 January 2026

This encompasses snow being eroded from the ground given strong enough wind shear, potentially getting mixed over deep layers, transported by the wind and deposited at sheltered locations (Mott et al., 2018).

These processes span a wide range of spatial scales. Erosional and depositional snow bedforms have scales of centimeters to several meters (Filhol and Sturm, 2015), and drifting snow leads to heterogeneities in snow height distribution at the scale of meters (Mott et al., 2011; Voordendag et al., 2024), while suspended snow may be transported over distances of hundreds of meters. Therefore even simulations at resolutions of five meters may not represent processes at all relevant scales (Mott and Lehning, 2010). However, major slope-scale patterns of redistribution can be captured with resolutions on the order of tens of meters (Mott and Lehning, 2010; Voordendag et al., 2024). Additionally to the mere mass redistribution effect of drifting and blowing snow, sublimation from airborne snow particles and the resulting cooling and moistening effect on the surrounding atmosphere (Groot Zwaaftink et al., 2011; Lundquist et al., 2024; Reynolds et al., 2024; Saigger et al., 2024; Sigmund et al., 2025) can have substantial influence. Apart from that, alternation of the snow surface structure due to drifting snow (Filhol and Sturm, 2015) has been shown to influence near-surface patterns of air flow and turbulent exchange, as well as subsequent snow redistribution patterns (Mott et al., 2010; Vionnet et al., 2013; Amory et al., 2017). In the past, modeling approaches to represent drifting snow have been implemented with various degrees of complexity, spanning from empirical, diagnostic and one-dimensional approaches (e.g., Liston and Sturm, 1998; Déry and Yau, 1999; Winstral and Marks, 2002; Warscher et al., 2013) to drifting snow modules integrated into numerical atmospheric models (e.g., Sauter et al., 2013; Vionnet et al., 2014; Sharma et al., 2023; Saigger et al., 2024)

In glaciological contexts, redistribution of snow by wind and avalanches has long been recognized as an important contributor to glacier mass balance (Cuffey and Paterson, 2010; Sauter et al., 2025). For example, Terleth et al. (2023) found that drifting snow contributes 18.7% to the winter mass balance of Storglaciären, Sweden. Temme et al. (2023) could improve their surface mass balance simulations in Cordillera Darwin, Chile, when including a simple redistribution scheme. On the other hand, drifting snow sublimation has been shown to be the dominant ablation term for glaciers in Pascua Lama, Dry Andes of Chile (Gascoin et al., 2013). Locally, surface albedo and thus energy balance is highly influenced by the presence of snow on the surface (Cuffey and Paterson, 2010) and therefore can be changed by exposing or covering bare ice due to redistributed snow. Despite this importance, most recent studies with distributed energy and mass balance models neglect redistribution of snow (e.g., Mortezapour et al., 2020; Blau et al., 2021; Abrahim et al., 2023; Khadka et al., 2024; Noël et al., 2025; Oulkar et al., 2025). However, even when including drifting snow in mass balance calculations, lacking detail in the wind field can still cause large differences between measured and modeled snow accumulation (Lambrecht and Mayer, 2024; Temme et al., 2025).

The availability of high-resolution wind fields poses a major challenge in modeling wind-driven redistribution and snow fall heterogeneity in mountain environments. Nested large-eddy simulations (LES) were proven to successfully represent wind systems in complex terrain (e.g., Umek et al., 2021; Goger et al., 2022) and to capture the interaction with snow redistribution and precipitation mechanisms (Vionnet et al., 2017; Gerber et al., 2018, 2019; Voordendag et al., 2024). However, due to the high computational demands this approach could only be applied to short case studies over small domain sizes. To circumvent this problem for longer analysis time frames, a number of approaches were introduced to predict high-resolution wind fields at low computational cost. These include e.g. extrapolation of observed wind based on topographic descriptors (Liston and Elder,

https://doi.org/10.5194/egusphere-2025-5608
Preprint. Discussion started: 16 January 2026

2006; Strasser et al., 2008; Schirmer et al., 2011) or wind library approaches with pre-computed wind fields from diagnostic downscaling tools like WindNinja (Wagenbrenner et al., 2016; Vionnet et al., 2021; Marsh et al., 2023) or numerical models under idealized atmospheric conditions (Dadic et al., 2010; Helbig et al., 2017, 2024). Reynolds et al. (2023) introduced HICAR as the high-resolution version of the Intermediate Complexity Atmospheric Research model (ICAR, Gutmann et al., 2016; Horak et al., 2021) building on linear mountain wave theory that achieves a speedup factor of 594 compared to numerical simulations with the Weather Research and Forecasting Model (WRF).

In recent years, machine learning (ML) methods have gotten large attention in the atmospheric sciences and specifically for downscaling tasks (Molina et al., 2023) due to their computational efficiency. For wind fields in mountain regions at meso-scale resolution such models have been introduced trained on operational numerical weather predictions (Miralles et al., 2022; Dupuy et al., 2023; Sekiyama et al., 2023). Dujardin and Lehning (2022) and Le Toumelin et al. (2023) developed ML-based downscaling models for near-surface wind in complex terrain at very high spatial resolution of 50 and 30 m, respectively. For this, Dujardin and Lehning (2022) trained their model on data from weather stations and high-resolution digital elevation models in Switzerland. The model of Le Toumelin et al. (2023) used the data set of idealized numerical simulations of Helbig et al. (2017) as training data. Despite the successful implementation, this model has the shortcomings of assuming a neutral stratification of the atmosphere, neglecting turbulent motions and assuming a linear dependence in the wind velocity.

Building on these recent developments, we present in this work a new downscaling model, that is tailored towards assessing near-surface winds and redistribution of snow in mountain environments and that addresses the shortcomings of earlier models. With our model, the snow drift sublimation and transport model (SNOWstorm), we specifically aim for these characteristics:

- parallel prediction of near-surface winds, snow mass change rate on the ground, sublimation from airborne snow particles and snow transport rate,
- large speed up rate compared to conventional numerical simulations of several orders of magnitude,
- direct applicability of the model over a wide range of regions world wide given only high-resolution terrain information and standard atmospheric input variables at large- to meso-scale resolution,
- representation of non-linear responses to changes in the atmospheric background conditions,
- representation of turbulent motions in the atmosphere,
- representation of interactions between drifting snow and the background atmosphere.

With these requirements in mind, we build a ML-based emulator model that is trained on a set of semi-idealized numerical simulations in LES setup which are representative for winter-time flow conditions in mountain environments. The paper is structured as follows: Section 2 introduces the training data set as well as the design and training of the ML model. Additionally, the approach to couple the trained model to coarse-scale atmospheric input is introduced here. The model is validated in Sect. 3. As a brief proof of concept we present in Sect. 4 a first real-world application of SNOWstorm in the European Alps revisiting the case study of Voordendag et al. (2024).

https://doi.org/10.5194/egusphere-2025-5608
Preprint. Discussion started: 16 January 2026

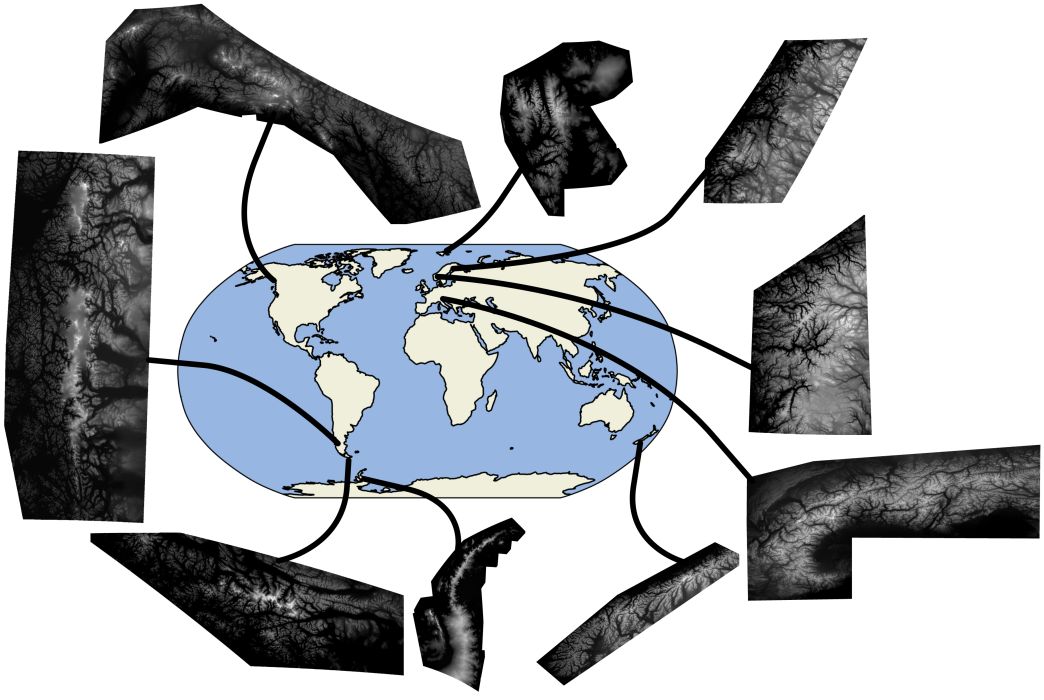

Figure 1. Overview map of regions used for the statistics in Sect. 2.1.1. Depicted are the terrain height as greyscale shading of DEM tiles cut to relevant topography.

2 Data and Methods

2.1 Training Data

The main goal of this work is to build a model that is applicable for a wide range of atmospheric conditions and over a wide range of regions. With this in mind the training data set comprises numerical simulations in a semi-idealized fashion with synthetic topographies and atmospheric conditions representative for a large number of glaciated mountain regions world wide, focusing on mid to high latitudes. The underlying idea is to capture the harmonics in the atmosphere-terrain interaction for terrain-induced flows with large-scale forcing. As described below in more detail, the synthetic topographies are therefore designed to reflect the range of spectral characteristics of real terrain. In the same way, the atmospheric conditions represent the range of harmonic properties found throughout winter-time mountain regions in mid- to high latitudes. The numerical simulations are run at very high resolutions ($\Delta x = 50$ m) in LES setup to explicitly resolve large turbulent motions and to capture relevant snow redistribution at slope scales. These numerical simulations are subsequently used as ground truth to train the ML model. The finished ML model can then be driven with input from large- to meso-scale atmospheric models and realistic topography.

https://doi.org/10.5194/egusphere-2025-5608
Preprint. Discussion started: 16 January 2026

2.1.1 Synthetic Terrain Generation

Work by Helbig and Löwe (2012) showed that essential characteristics of real terrain can be represented by artificial topographies such as Gaussian Random Fields. Atmospheric simulations run on such topographies can inform downscaling tools for, e.g., wind (Helbig et al., 2017; Le Toumelin et al., 2023). Our approach builds on this idea, but concentrates on the spectral characteristics of terrain as already been used in modeling approaches building on linear mountain wave theory (Smith and Barstad, 2004; Sauter, 2020). For this, we first analyze spectral slope characteristics of real terrain and subsequently use these characteristics to build a set of new, synthetic topographies.

We start by analyzing terrain for spectral slope characteristics following the same method as introduced by Young and Pielke (1983) with 2D-applications by Steyn and Ayotte (1985) and Salvador et al. (1999). First, 30 m resolution digital elevation models (DEMs) of the Copernicus DEM GLO-30 (European Space Agency, 2019) of the regions shown in Fig. 1 are resampled to 50 m horizontal resolution and cut to tiles of 256x256 points in order to fit the requirements of the later model. To avoid large spectral amplitudes at wavenumber 0, the deviation from a linearly fitted plane is calculated. Additionally, a cosine filter is applied on the outermost 10 grid points at each border to taper out the terrain in order to avoid discontinuities at the tile edges. On these filtered and de-trended DEMs a 2D Fast Fourier Transform (FFT) is applied (Cooley and Tukey, 1965). We take the module of the complex values and normalize by the domain size in order to get the amplitude spectrum A. Subsequently, the decay of spectral amplitude with increasing wavenumber k is described by the function

$$A = ak^b. \tag{1}$$

Here, stronger negative values of b indicate less spectral amplitude contained in smaller wave lengths and thus more smooth´ terrain. This procedure is applied to regions shown in Fig. 1, including mountain regions in North and South America, Scandinavia, the Alps, New Zealand, and the Antarctic Peninsula, as these are also regions for potential later applications of SNOWstorm. Figure 2 shows the distribution of spectral slopes for the analyzed mountain regions, with values resembling earlier studies (Young and Pielke, 1983; Steyn and Ayotte, 1985; Salvador et al., 1999). Statistics for the individual mountain ranges are very similar (not shown).

Our method to create new, synthetic topographies ("Fourier Land") builds on replicating the spectral slope characteristics described above. It is similar to the approach shown in Jacobs et al. (2017) for artificial surfaces in material sciences and methods used to create landscapes and water surfaces in movies and computer games. On a matrix of white noise a 2D FFT is applied, the amplitude is scaled following Eq. 1. After that an inverse FFT is applied to create the topography. In total a set of 72 topographies was created with values for a and b randomly drawn from values in the range of the ones observed in real terrain (Fig. 2). A small subset of example topographies with different spectral slope settings is shown in Fig. S1. These synthetic topographies are later used as terrain input for the numerical simulations. In order to avoid steep slope angles ($< 40°$) that would cause issues with numerical stability in the simulations, we omit the smallest negative values of $b > -1.7$ and very high values of $a > 18$. Very low values of $a < 13$ are also neglected, as these stem from tiles with almost flat topography. With this in mind, our topographies are slightly smoother than real topography and do not represent the extreme values in the

https://doi.org/10.5194/egusphere-2025-5608
Preprint. Discussion started: 16 January 2026

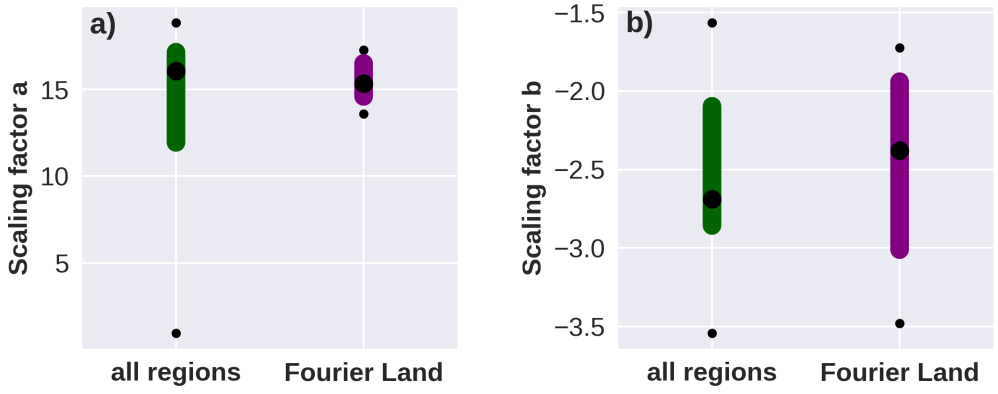

Figure 2. Distribution of factors a and b from Eq. 1 for topography tiles from selected regions ("all regions", see Fig. 1) and synthetic topographies ("Fourier Land"). Depicted are median (large dot), 10th and 90th percentile (range of colored bar) and minimum and maximum value (small dot) of the distribution.

variability of slope angles as well as of other commonly used terrain descriptors like topographic position index (TPI, Weiss, 2001), maximum upwind slope angle (Winstral et al., 2002) or the terrain curvature (not shown).

2.1.2 Numerical model

In order to create the training data set, simulations with the Weather Research and Forecasting (WRF) model (Skamarock et al., 2019) are conducted. We use the Advanced Research WRF version 4.3.1 with the coupled snow drift module of Saigger et al. (2024) and online LES diagnostics WRFlux, version 1.3.2 of Göbel et al. (2022). Each model domain consists of 256x256 grid points with a horizontal grid spacing of $\Delta x = 50\ \mathrm{m}$ and 81 terrain-following vertical levels. The lowest mass point is located at approximately 10 m above the ground, the model top is set to 12000 m with Rayleigh damping activated for the upper 5000 m.

With the ideal-case setup of our simulations, only a reduced number of physical parameterizations is used. No parameterizations for radiative transfer or microphysics are employed. We use the Revised MM5 surface layer scheme (Jiménez and Dudhia, 2012) and the scale-adaptive sub-grid scale turbulent closure scheme (SMS-3DTKE) of Zhang et al. (2018) (km_opt = 5) blending between LES with the turbulence closure of Deardorff (1980) and the PBL-scheme of Nakanishi and Niino (2006) at the meso-scale limit. No land-surface parameterization is employed which also means that no explicit treatment of snow processes on the ground is in place. Instead we define a "passive" snow layer with prescribed thickness and density that only experiences wind-driven erosion or deposition. All simulations employ the drifting snow scheme of Saigger et al. (2024), in which snow erosion depends on snow density and surface shear stress. Airborne snow is transported by the resolved three-dimensional wind and parameterized turbulent mixing with a super-imposed particle subsidence. In our simulations, sublimation from drifting snow particles and its cooling and moistening effect on the ambient atmosphere is represented; the surface particle radius is set to $2 \cdot 10^{-4}\ \mathrm{m}$.

https://doi.org/10.5194/egusphere-2025-5608
Preprint. Discussion started: 16 January 2026

Table 1. Range of atmospheric input variables to drive the numerical simulations

variable	min. value	max. value
wind speed ($\mathrm{m\ s^{-1}}$)	0	30
wind direction (deg)	0	359
Brunt-Väisälä Frequency ($\mathrm{s^{-1}}$)	0	0.019
ground-level pressure (hPa)	600	1000
ground-level temperature (K)	245	285
ground-level relative humidity ($\%$)	40	99
roughness length (m)	0.0001	0.002
snow/ice density ($\mathrm{kg\ m^{-3}}$)	50	915

In total we run 720 individual simulations. For each simulation the terrain height is defined by one of the artificial topographies described above, which means that ten simulations with different atmospheric conditions are conducted on each topography. All simulations are initialized with horizontally homogeneous profiles of potential temperature, specific humidity and the meridional and zonal wind component. These profiles are calculated from values of wind speed and direction, static stability, expressed as Brunt-Väisällä Frequency, and ground-level pressure, temperature and relative humidity. Values for pressure, temperature and humidity are taken randomly from within the ranges described in Tab. 1, reflecting the variability over winter-time mountain environments. For each simulation a unique combination of wind speed and stability, ranging from neutral to isothermal conditions, is drawn, while the wind direction is shifted by one degree with each simulation. Note that initial profiles of wind speed, direction, stability, and relative humidity are vertically constant, neglecting e.g. conditions with vertical wind shear or variations in stability. In order to ensure that snow is continuously present on the ground for the entire simulation period, it is initialized with a thickness of $1\ \mathrm{m}$. Snow density is drawn randomly from the range of plausible values (very low-density snow to ice density) with the distribution skewed towards fresh-snow densities. The roughness length is set constant over each domain with values representing snow-covered surfaces (Tab. 1, Fitzpatrick et al., 2019).

We run the simulations with a time step of $0.5\ \mathrm{s}$ until the near-surface turbulent fluxes have stabilized. We then use the stabilized, quasi-steady state fields as training data for the machine learning model. Our synthetic topographies are periodic by design, which allows us to employ periodic boundary conditions. These lead to a quick convergence of the turbulent fluxes throughout the entire domain without the need of buffer zones or perturbations at the domain boundaries (e.g., Krieger et al., 2025). Visual inspection showed that turbulent fluxes stabilized within the first three to four hours of model run time, in line with earlier ideal-case atmospheric simulations (e.g., Kirshbaum and Durran, 2004). Thus, all simulations were run for six hours with the first four hours disregarded as spin-up and the averaged and accumulated fields of the last two hours used for later training.

https://doi.org/10.5194/egusphere-2025-5608
Preprint. Discussion started: 16 January 2026

2.2 SNOWstorm

2.2.1 Basic design and data handling

In the past, convolutional neural networks (CNNs) have proven to successfully identify spatial structures especially in gridded data (LeCun et al., 2015). Building on that, we use the U-Net (Ronneberger et al., 2015) as the basic architecture in our study. U-Nets are fully convolutional networks that were first introduced for image segmentation, but have also been successfully applied for model emulating tasks in atmospheric sciences (e.g., Dupuy et al., 2023; Höhlein et al., 2020; Le Toumelin et al., 2023; van der Meer et al., 2023). Typically, U-Nets consist of an encoder path and a decoder path. In the encoder path, blocks of convolutional layers (in our case 3x3 convolution kernels with stride of 1 and circular padding, Fig. 3) and non-linear activation functions (in our case leakyReLU), followed by pooling layers (in our case 2x2 Max Pooling with stride of 2) are used to encode spatial patterns with increasing levels of abstraction and decrease the spatial resolution of the data. After each pooling layer, the number of feature maps is increased to compensate for the loss in spatial information. In the decoder path, blocks of up-sampling operations, followed by convolutional layers and non-linear activation functions are used to reconstruct high-resolution relationships. Additionally, skip connections are employed, where information is directly passed from the encoder path to the decoder path in order to preserve high-resolution spatial information. In total, our U-Nets consist of each four encoder and decoder blocks and a bottleneck of dimensions 16x16x512 (Fig. 3).

We train a separate U-Net for each of our four predictants (near-surface winds (NSW), snow mass change rate (DSM), vertically integrated sublimation rate (SUBL_VI), vertically integrated snow transport rate (SNOW_VI, vertically integrated product of snow particle mass concentration and wind vector). We use the high-resolution field of terrain height as predictor and the low-resolution atmospheric fields and surface values (snow density ρ_{snow}, roughness length μ, offset elevation z_0) that the WRF simulations were driven by (Fig. 3). The atmospheric fields include above-crest height values of wind components (u, v), static stability expressed as Brunt-Väisällä Frequency (N), and surface-level values of air pressure (p), temperature (T), and relative humidity (rH). In addition to the terrain height we provide extra terrain information as a predictor similar to previous work (Dujardin and Lehning, 2022; Dupuy et al., 2023). Here we provide cos_{a-d}, the cosine of the difference angle between the ambient wind direction and the local slope aspect angle to indicate slopes exposed and sheltered from the ambient wind. Apart from that, the predictions of NSW are given as an additional predictor to the other U-Nets. This stacking of the ML-models drastically improved the learning process in the snow-related models.

We perform a z-score normalization on all input and output fields. In order to deal with the skewness in the distributions additional log-transformations were applied for DSM and SUBL_VI as well as a square-root transformation on the terrain height and for SNOW_VI.

2.2.2 Training

The most important hyperparameters for the model training are summarized in Table S1. For all but SNOW_VI the mean squared error (MSE) was used as the loss function. Here, the mean absolute error (MAE) proved more successful. During

https://doi.org/10.5194/egusphere-2025-5608
Preprint. Discussion started: 16 January 2026

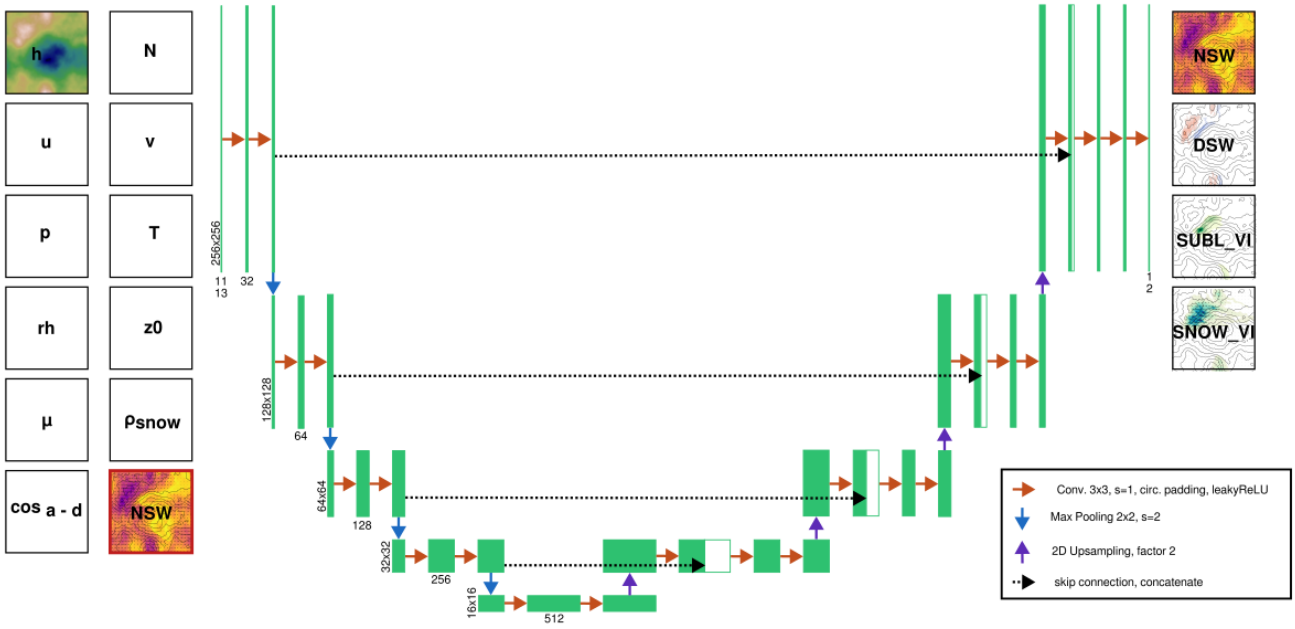

Figure 3. Schematic depiction of the U-Net architecture used for individual SNOWstorm model components. Green blocks and numbers indicate dimensions of feature maps, arrows show the individual operations. Squares on the left and right side symbolize the different input and output fields of the model (only one of the output fields for each U-Net, near-surface wind (red square) used as additional input in U-Nets for DSM, SUBL_VI, and SNOW_VI). The output for NSW and SNOW_VI has dimensions 2x256x256 as the components in x and y direction are predicted separately.

model development we tested to include penalty terms in the loss function to ensure mass conservation between DSM and SUBL_VI. However, dividing into separate U-Nets for DSM and SUBL_VI and using the MSE provided better results.

We split the data set in test (1/8, 90 samples: all respective simulations over 9 randomly drawn topographies), validation (1/8) and training (6/8). With the periodic nature of our data, we are able to employ data augmentation by shifting the fields in x or y direction by a random distance (Goodfellow et al., 2016), which much improved model robustness. Other commonly used data augmentation techniques like rotating, flipping, linear rescaling or splitting of the data were deemed impractical for our applications. Thus, in each training epoch, the training set is once presented in unchanged form and once with each sample shifted by a random distance. The individual models are trained until convergence is reached and no indications of overfitting are present (Goodfellow et al., 2016) (Fig. S2).

2.3 Coupling with real-world atmospheric input

We provide a coupling module to run SNOWstorm with real-world atmospheric input. This extracts relevant fields from the atmospheric input data sets and brings them into a form usable for SNOWstorm. Here we provide routines for coupling to data

https://doi.org/10.5194/egusphere-2025-5608
Preprint. Discussion started: 16 January 2026

from ERA5 and WRF, however, driving SNOWstorm with other datasets of, e.g., regional reanalyses is theoretically possible. A DEM has to be provided at a spatial resolution of 50 m. All subsequent steps are performed on the spatial grid of this DEM. To be consistent with the training data, the elevation of the lowest point in the domain is subtracted from the DEM and a square-root filter is applied, the offset elevation (z_0) is given to SNOWstorm as an additional input field. Above-crestheight wind and stability are extracted and calculated at defined pressure levels (default: 600 hPa for wind and layer between 600 and 500 hPa for stability.) All ground-level input fields (pressure, temperature, relative humidity) are extracted at the ground level of the input atmospheric data set. Subsequently, pressure is reduced from the elevation of the input data set terrain to the offset elevation z_0 using the hydrostatic equation. Temperature is reduced with a moist-adiabatic lapse rate of $\Gamma_m = 0.0065\ \mathrm{K\ m^{-1}}$, while relative humidity stays unchanged. All extracted and calculated fields are then interpolated to the grid of the fine-scale DEM. In the current version of SNOWstorm, snow density and aerodynamic roughness length have to be provided and are then constant throughout the domain. The SNOWstorm-predicted fine-scale near-surface wind field is provided as additional input for the predictions of DSM, SUBL_VI and SNOW_VI. Before the call of SNOWstorm, all input fields are normalized with the normalization factors derived during training; output fields are back-transformed accordingly.

In the example case of Sect. 4 we use this coupling strategy with specifications for individual experiments as described in Sect. 4.2.

3 Validation of SNOWstorm

3.1 Cross validation

To provide an overview on the performance of SNOWstorm, we show examples of SNOWstorm predictions for select cases in the test data set, unseen during training and results from cross validation experiments. We run a six-fold cross validation for all individual ML-models. Here we compute the error between the SNOWstorm-predicted fields and the corresponding WRF fields at grid-cell scale. Additionally, we divide the errors into classes of wind speed based on the WRF-predicted wind speed. Overall mean absolute errors in wind speed are around 0.8 $\mathrm{m\ s^{-1}}$, with a bias of -0.12 $\mathrm{m\ s^{-1}}$ and a Pearson correlation coefficient of 0.94 (Fig 4 a – c). The spread over the individual cross validation experiments is low with the MAE between 0.75 and 0.87 $\mathrm{m\ s^{-1}}$, the bias between -0.06 and -0.22 $\mathrm{m\ s^{-1}}$, and correlation coefficient between 0.92 and 0.95. With increasing wind speed also the mean error increases up to about 1.5 $\mathrm{m\ s^{-1}}$ for grid cells with wind speed higher than 10 $\mathrm{m\ s^{-1}}$. For the slowest velocity class below 1 $\mathrm{m\ s^{-1}}$ SNOWstorm overestimates the wind speed by 0.16 $\mathrm{m\ s^{-1}}$, while for all other velocity classes we observe a negative bias. This indicates that the wind fields predicted by SNOWstorm are slightly too smooth and the full range of velocity can not be represented. Pattern correlation for the individual velocity classes decreases to values around 0.7 and to 0.35 for grid cells with WRF wind speeds below 1 $\mathrm{m\ s^{-1}}$ (Fig. 4 c). Compared to the high correlation over the entire velocity range this indicates that the overall velocity distribution is captured, while local details in the wind field might be missing. As will be seen in the example cases below, SNOWstorm especially struggles to capture the flow structure in weak-wind wake regions which is reflected in the low correlation in the lowest velocity class. With increasing wind speeds the

https://doi.org/10.5194/egusphere-2025-5608
Preprint. Discussion started: 16 January 2026

spread between the individual experiments increases in all error measures. This might point to a comparatively small sample size and a dependence of the performance on only a few cases.

The errors in these experiments fall in line with errors reported in comparable studies. Le Toumelin et al. (2023) report for their ML model (trained on simulated data over synthetic topographies) an MAE of 0.16 $\mathrm{m\,s^{-1}}$, a bias below 0.01 $\mathrm{m\,s^{-1}}$, and a correlation coefficient of 0.96 in their cross validation experiments. Dujardin and Lehning (2022) find for their model (trained on weather station data and high-resolution terrain descriptors) a MAE of 1 to 1.5 $\mathrm{m\,s^{-1}}$ with a negative bias between -0.16 and -0.04 $\mathrm{m\,s^{-1}}$ depending on surrounding terrain characteristics. Correlation coefficients here range between 0.42 and 0.66. Errors in the model of Dupuy et al. (2023) with a target resolution of 1 km are in a comparable range with a MAE of about 0.7 $\mathrm{m\,s^{-1}}$ and a bias of -0.01 $\mathrm{m\,s^{-1}}$. While being in a similar range all these comparisons have to be made with caution, given the different target resolutions, and different nature and degree of complexity in the respective training data.

Errors for the predicted rates of snow mass change, sublimation, and snow transport show a very similar behavior as the errors of the wind field. Overall MAE for DSM is at 0.2 $\mathrm{kg\,m^{-2}\,h^{-1}}$ increasing from about 0.11 $\mathrm{kg\,m^{-2}\,h^{-1}}$ in the lowest velocity class to about 0.5 $\mathrm{kg\,m^{-2}\,h^{-1}}$ for grid cells with highest wind speeds (Fig. 4 d). MAE for the sublimation rate are in a similar range with 0.16 $\mathrm{kg\,m^{-2}\,h^{-1}}$ for all grid cells and increasing from 0.12 to 0.28 $\mathrm{kg\,m^{-2}\,h^{-1}}$ in the highest velocity class. Similarly, MAE for SNOW_VI increases from 0.06 to 2.59 $\mathrm{kg\,m^{-1}\,s^{-1}}$ in the highest velocity class with 0.73 $\mathrm{kg\,m^{-1}\,s^{-1}}$ overall. Similar to the wind velocity, DSM, SUBL_VI, and SNOW_VI are slightly overestimated in the low velocity classes and underestimated for cells with increasing wind speed. The overall bias is close to zero (DSM: -10^{-3} $\mathrm{kg\,m^{-2}\,h^{-1}}$, SUBL_VI: -$10^{-4}$ $\mathrm{kg\,m^{-2}\,h^{-1}}$, SNOW_VI: 0.17 $\mathrm{kg\,m^{-1}\,s^{-1}}$). Correlation is generally lower compared to the predictions of wind speed and with a large spread over the experiments again possible problems with too small sample sizes (Fig. 4 f, i, l).

3.2 Performance on example data sets

The following three example cases are selected to represent different atmospheric conditions that SNOWstrom is trained for and showcase the performance on different flow patterns. Two cases have relatively high wind speeds and thus considerable amounts of snow redistribution (case A: Fig. 5, case B: Fig. 6), while the third one only experiences very low wind speeds and consequently no drifting snow is present (case C: Fig. S3). With the ambient relative humidity well below saturation (70%) in case A, sublimation from drifting snow particles plays a crucial role here, while high relative humidity in case B suppresses sublimation.

The wind fields predicted by SNOWstorm in general agree with the WRF-simulated flow fields. SNOWstorm captures the overall wind direction and speed as well as terrain-induced flow features such as acceleration at ridges, and deflection and channeling around summits, and through gaps and valleys (Figs. 5, 6, S3, b–c). While capturing the general patterns in regions of lee-side flow separation (case A and C), SNOWstorm can not fully reproduce the associated sharp gradients in wind velocity as well as flow patterns in the weak-wind wake regions.

Similar to the wind fields, patterns in snow erosion and deposition generally agree with the WRF simulations. The placement of zones of erosion and deposition as well as the overall amounts in these zones fit well in cases A and B (Fig. 5, 6 d–e). However, the maximum amounts of snow deposition (e.g., in the lee of the northern hill in case A, secondary patches in case B)

https://doi.org/10.5194/egusphere-2025-5608
Preprint. Discussion started: 16 January 2026

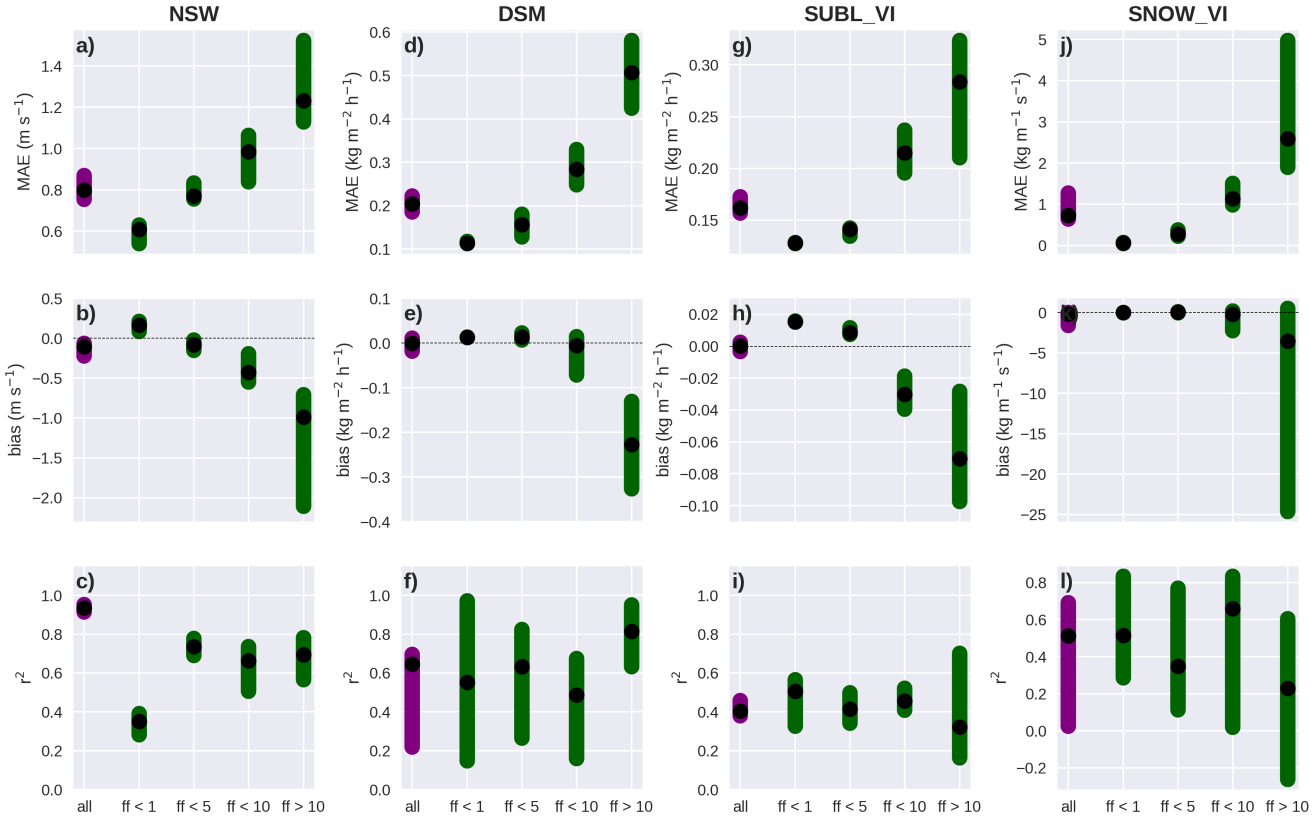

Figure 4. Grid-cell wise mean absolute error (MAE), bias, and squared Pearson correlation coefficient (r^2) for cross validation experiments. Errors are depicted for wind speed (a–c), snow mass change rate (d–f), sublimation rate (g–i) and integrated snow transport (j – l to be done). Black dots and colored bars denote the median and range over the cross validation experiments. Purple bars show results for all points, green bars for points in classes of wind speed as indicated on the x axis (wind speed (ff) < 1 m s^{-1}, 1 m s^{-1} < ff < 5 m s^{-1}, etc.). Black dashed lines in b, e, h, and k indicate the bias of 0.

https://doi.org/10.5194/egusphere-2025-5608
Preprint. Discussion started: 16 January 2026

are underestimated by SNOWstorm. In the weak-wind case C, SNOWstorm successfully predicts very low snow mass change rates below our threshold of depiction in the figure (Fig. S3 d–e). However, due to its design, SNOWstorm does not recognize zero as a special value, and thus, will not necessarily predict values of exactly zero but small values close to zero in situations where no snow redistribution should occur. Over long integration time scales these small errors might become significant, so future users should consider applying zero filters for very small values. This is also true for situations of no relevant drifting snow sublimation (case B, C, Figs. 6, S3 f–g): SNOWstorm successfully predicts values very close to zero, though not exactly zero. In the case A with sublimation playing an important role, SNOWstorm manages to predict the basic placement and amount of drifting snow sublimation (Fig. 5 f–g). Predictions of the snow transport rate are in line with the results of the other model components: the overall shape and amounts are captured by SNOWstorm, while the zones of maximum snow transport are slightly underestimated and slightly misplaced.

In summary, wind fields predicted by SNOWstorm generally agree with the LES ground truth, except for highly turbulent flow features such as lee-side flow separations and in wake regions. Predictions of snow redistribution and sublimation as well fit to the WRF simulations. Mismatches in the simulated flow field can influence predictions of snow-related fields.

4 Case study: application of SNOWstorm

4.1 Case study overview

To provide a short outlook on potential applications of SNOWstorm, we revisit the case study of 8 February 2021 on Hintereisferner, a glacier in the Austrian Alps, studied in detail by Voordendag et al. (2024). Figure. 7 provides an overview for the region and available weather stations. The event was characterized by a cold front passage during the night with fresh snowfall and a subsequent increase and shift in wind, leading to large amounts of snow redistribution in the second half of the day. The amounts of snowfall and redistribution were observed by three terrestrial laser scans. Additionally, nested large-eddy simulations at $\Delta x = 48$ m in WRF (HEF-LES) with the coupled snow drift scheme of Saigger et al. (2024) were performed. Validation of wind speeds and direction against three automated weather stations (Fig. 7 for location) showed a remarkable accuracy of the simulated flow field. Comparison to the observed snow height change revealed that the overall amounts and slope-scale patterns of snow redistribution are captured well in the LES, while smaller-scale patterns are not represented. For more details in the methods and results we refer to the original publication of Voordendag et al. (2024).

4.2 Experiment setup

To better understand the behavior of SNOWstorm in real-world applications, experiments with different coupling strategies as described below and summarized in Table 2 are run and validated against the results of the HEF-LES as well as against the observations from the weather stations. The coupling to the atmospheric input is done following the procedure described in Sect. 2.3. To understand the influence of meso-scale atmospheric information we perform experiments driving SNOWstorm with input taken from ERA5 and the two outer domains of the WRF simulations of Voordendag et al. (2024) D01 ($\Delta x = 6$ km)

https://doi.org/10.5194/egusphere-2025-5608
Preprint. Discussion started: 16 January 2026

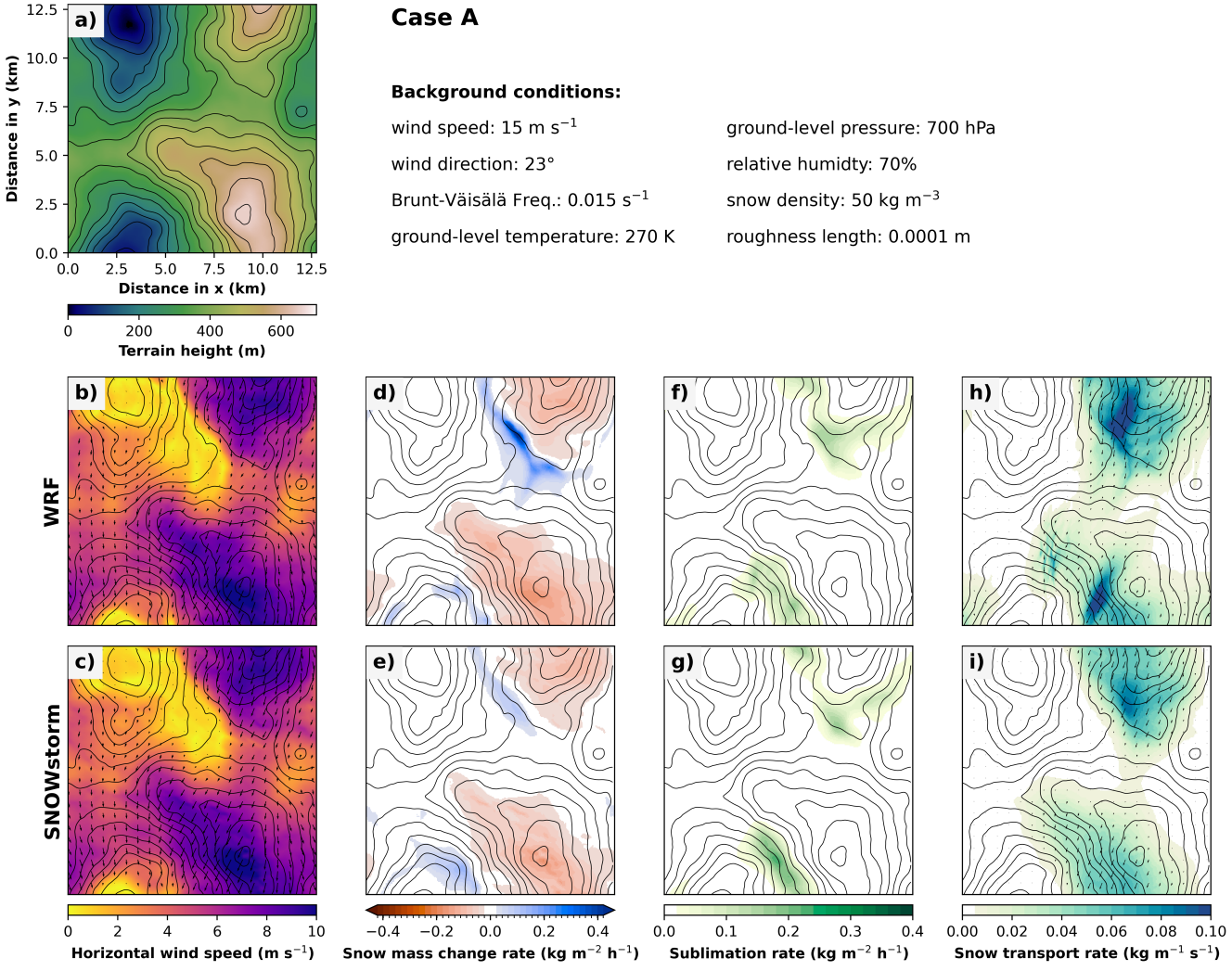

Figure 5. Example case A of SNOWstorm predictions (lower row) and WRF ground truth (middle row). Depicted are model terrain height (a), 10 m flow field (b–c), snow mass change rate (d–e), drifting snow sublimation rate (f–g) and integrated snow transport rate (h–i, arrows and colors). Model terrain height is additionally indicated by black contour lines with an interval of 100 m. Background conditions for each case are specified in the upper row. The case is part of the test data set, unseen during training.

https://doi.org/10.5194/egusphere-2025-5608
Preprint. Discussion started: 16 January 2026

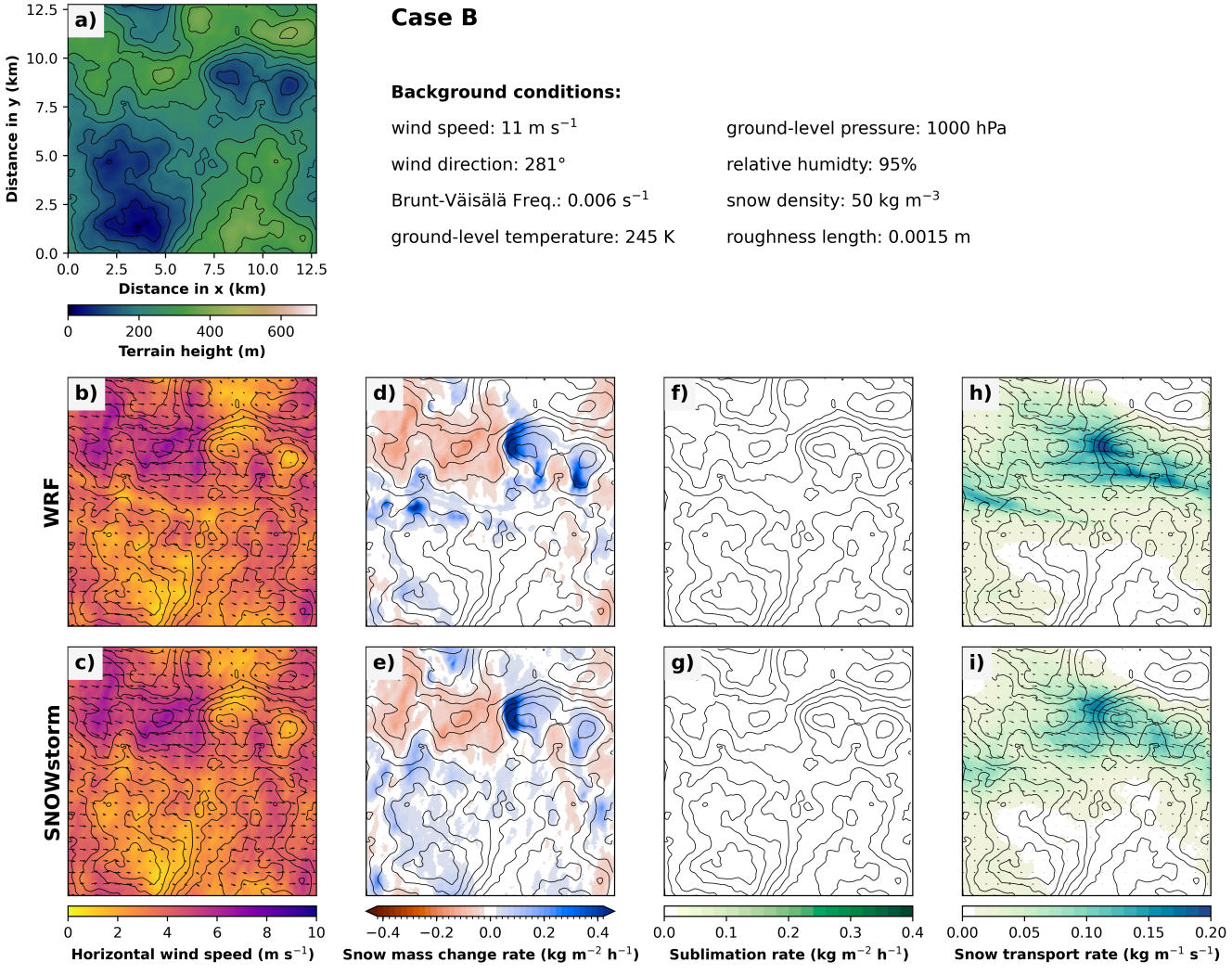

Figure 6. Similar to Fig. 5, but for case B. Note the changed colorscale for terrain height and integrated snow transport rate.

https://doi.org/10.5194/egusphere-2025-5608
Preprint. Discussion started: 16 January 2026

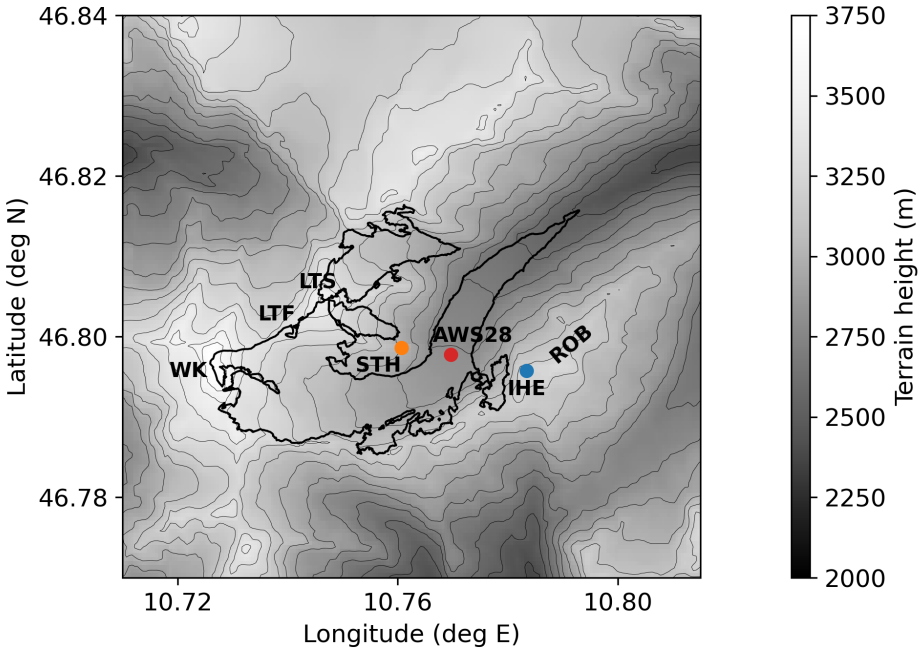

Figure 7. Overview map of Hintereisferner. Depicted are terrain height as contour colors and black contour lines (line spacing 100 m), the outlines of Hintereisferner glacier as tick black lines, and the location of weather stations as colored dots (Im Hinteren Eis (IHE), Station Hintereis (STH), temporary station on the glacier (AWS28)). Important landmarks are indicated by their abbreviations (Weißkugel (WK), Rofenberg (ROB), Langtauferer Ferner glacier (LTF), Langtauferer Spitze (LTS)).

and D02 ($\Delta x = 1.2$ km). Additionally, we run experiments with the smoothed digital elevation model used in the HEF-LES and with the un-smoothed DEM of GLO-30, resampled to $\Delta x = 50$ m (see Tab. 2 for overview of experiment settings).

For the experiments we do not couple SNOWstorm to any snow model but prescribe a snow density (200 kg m^{-1}) and roughness length (0.1 mm) consistent with the ones in the HEF-LES. Given the short duration of the case study, we consider this reasonable. However, for future long-term investigations, coupling to a snow model will be necessary.

4.3 Case study results

We will first focus on the second half of the day (after 14 UTC), the phase with highest wind speeds and snow redistribution taking place. Here, SNOWstorm driven with input from the two meso-scale domains (S_WD1_W and S_WD2_W, Tab. 2) predicts flow fields that are in agreement with the HEF-LES (Fig. 8 b–d, Fig. 9). While slightly smoother, terrain effects like flow acceleration and deflection around ridges and mountain tops, as well as leeside effects are represented by SNOWstorm. Predicted wind velocities at the three observation sites (Station Hintereis (STH), Im Hinteren Eis (IHE), temporary station on

https://doi.org/10.5194/egusphere-2025-5608
Preprint. Discussion started: 16 January 2026

the glacier (AWS28), see Fig. 7 for locations) generally fit well to the measurements with absolute errors on the order of 1 – 4 $\mathrm{m\,s^{-1}}$ (Tab. 3). Errors at IHE and AWS28 mainly stem from an overall overestimation of wind speed by SNOWstorm.

The channeling effect inside the valley is less pronounced in SNOWstorm, leading to a too strong westerly component and an offset in wind direction here. While SNOWstorm predictions in S_WD1_W and S_WD2_W show similar results, the experiments with ERA5 input (S_ERA_W) capture the overall flow structure, though with generally too weak winds (Fig. 8 a, Fig. 9, Tab. 3). This indicates that the meso-scale flow accelerations, that is lacking in ERA5, is necessary for SNOWstorm to capture strength of the local flow field. Apparently, the meso-scale flow structure is already represented enough in the WRF D01, and no additional information is provided by the finer input data. Nevertheless, at specific locations (IHE and AWS28) S_ERA_W outperforms the experiments with meso-scale input (Tab. 3). The experiments with SNOWstorm driven on the unsmoothed GLO-30 topography show similar structures (Fig. S3), which is remarkable, as the steepest slope angles here exceed all slope angles seen during training. With the finer structure in this topography also finer features in the wind field, e.g., around secondary ridge lines can be simulated.

In the first half of the day, SNOWstorm fails to capture the weak northerly flow caused by shallow cold-air inflow and overspill after the frontal passage. During the transition phase around 12 UTC SNOWstorm predicts the increase in wind speed about three hours too early (Fig. 9) which consequently causes a too early onset of snow redistribution and increased errors when considering the full day (Tab. 3). Both effects are explainable as SNOWstorm has the assumption that the local wind field adapts instantaneously to changes in the large-scale forcing and effects of shallow cold air advection and cold air pools have not been seen in training.

Consistent with the wind predictions, accumulated snow mass changes simulated by SNOWstorm (S_WD1_W and S_WD2_W) generally agree well with the ones in the HEF-LES (Fig. 8 f–h). Maximum snow erosion is predicted at the summit region of Weißkugel, and at the ridges north-west and south-east of Hintereisferner. Regions of maximum erosion are slightly more localized with slightly higher amounts in the HEF-LES. Apart from that, erosion zones are shifted from the ridge more towards the lee-side slopes at several places (Langtauferer Spitze, Rofenberg, see Fig. 7 for location). Due to the high overall wind speeds only very few regions of snow deposition are simulated in the HEF-LES as well as by SNOWstorm. These include especially the upper part of Langtauferer Ferner and the area around AWS28 at several instances in time in phases of stronger lee-side deceleration. The deposition zone in the lee of Rofenberg simulated in HEF-LES is not captured by SNOWstorm due to the high wind velocities here. Consistent with the too low wind velocities, SNOWstorm simulates a much smaller change in snow mass in the experiment S_ERA_W (Fig. 8 e). As already seen for the wind field, the experiments with GLO-30 topography show similar results, though with smaller-scale features captured by the more detailed input topography (Fig. S3). Sublimation from drifting snow particles plays a negligible role in both modeling approaches (Fig. S4). Similar to the other variables, the overall amounts and the placement of sublimation zones predicted by SNOWstorm generally agree with the ones simulated in HEF-LES.

In summary, SNOWstorm manages to capture the general shape and strength of the flow field as well as the overall amounts and location of snow redistribution during this case study. Local details in the flow field and transition periods in the large-scale forcing remain challenging for SNOWstorm. The large advantage of the ML model, however, lies in its computational

https://doi.org/10.5194/egusphere-2025-5608
Preprint. Discussion started: 16 January 2026

Table 2. Summary of input data for the different real-case experiments presented. Each experiment abbreviation consists of the model used (SNOWstorm: S), the atmospheric input data (ERA5: ERA, WRF D01: WD1, WRF D02: WD2) and the topographic input data (GLO-30: G, smoothed HEF-LES topography: W)

	S_ERA_W	S_ERA_G	S_WD1_W	S_WD1_G	S_WD2_W	S_WD2_G
atmospheric input	ERA 5	ERA 5	WRF D01	WRF D01	WRF D02	WRF D02
topographic input	HEF-LES	GLO-30	HEF-LES	GLO-30	HEF-LES	GLO-30

Table 3. Error statistics with MAE and bias of SNOWstorm predictions (first value: S_ERA_W, second value: S_WD1_W, third value: S_WD2_W) validated against observations at Station Hintereis (STH), Im Hinteren Eis (IHE) and station on the glacier (AWS28) and point-wise against HEF-LES for the phase of strongest winds (after 14 UTC) and the full day.

		STH	IHE	AWS28	HEF-LES
after 14 UTC	MAE wind speed ($\mathrm{m\ s^{-1}}$)	3.11 / 1.56 / 1.96	3.80 / 3.52 / 4.43	2.46 / 3.77 / 3.40	4.35 / 3.81 / 3.92
	bias wind speed ($\mathrm{m\ s^{-1}}$)	-2.39 / 0.32 / -0.84	-1.17 / 3.04 / 4.43	-2.28 / 3.77 / 3.40	-3.53 / -0.09 / -0.03
full day	MAE wind speed ($\mathrm{m\ s^{-1}}$)	6.00 / 3.10 / 3.10	2.55 / 4.02 / 3.93	1.69 / 4.09 / 3.71	5.71 / 3.78 / 3.61
	bias wind speed ($\mathrm{m\ s^{-1}}$)	-6.00 / 2.52 / 1.80	-1.17 / 3.80 / 3.89	-1.37 / 4.09 / 3.71	-5.08 / -0.42 / 0.06

efficiency: the computations for the nested LES of Voordendag et al. (2024) required about 10^4 core hours. In contrast, the predictions with SNOWstorm can be run on a single CPU in 4 s for the entire day with ERA-5 input and 0.1 and 0.3 h, respectively, with WRF input due to the longer processing time during input data preparation. This means a speedup factor on the order of 10^5 to 10^7 and reasonable computational demands for simulations over entire accumulation seasons.

5 Conclusions and Outlook

In this work we introduced SNOWstorm as a new, deep-learning based emulator model for near-surface winds and snow redistribution in mountainous terrain at high spatial resolutions ($\Delta x = 50\ \mathrm{m}$). The model has a U-Net architecture and is trained on output of semi-idealized numerical simulations with synthetic topographies and atmospheric conditions representative for a wide range of regions world wide.

We performed validation experiments and applied the model on a short case study in the European Alps comparing to observations and nested Large-Eddy simulations (LES). Key findings from the validation experiments are:

- SNOWstorm in general successfully predicts the overall spatial distribution and strength of the flow field with terrain-induced flow modifications. Position and amounts of zones of snow erosion, deposition, sublimation, and snow transport agree with the ground truth.
- Highly turbulent flow features and sharp gradients pose a challenge to the ML-model. Mispredictions in the wind field can further influence snow-related predictions.

https://doi.org/10.5194/egusphere-2025-5608
Preprint. Discussion started: 16 January 2026

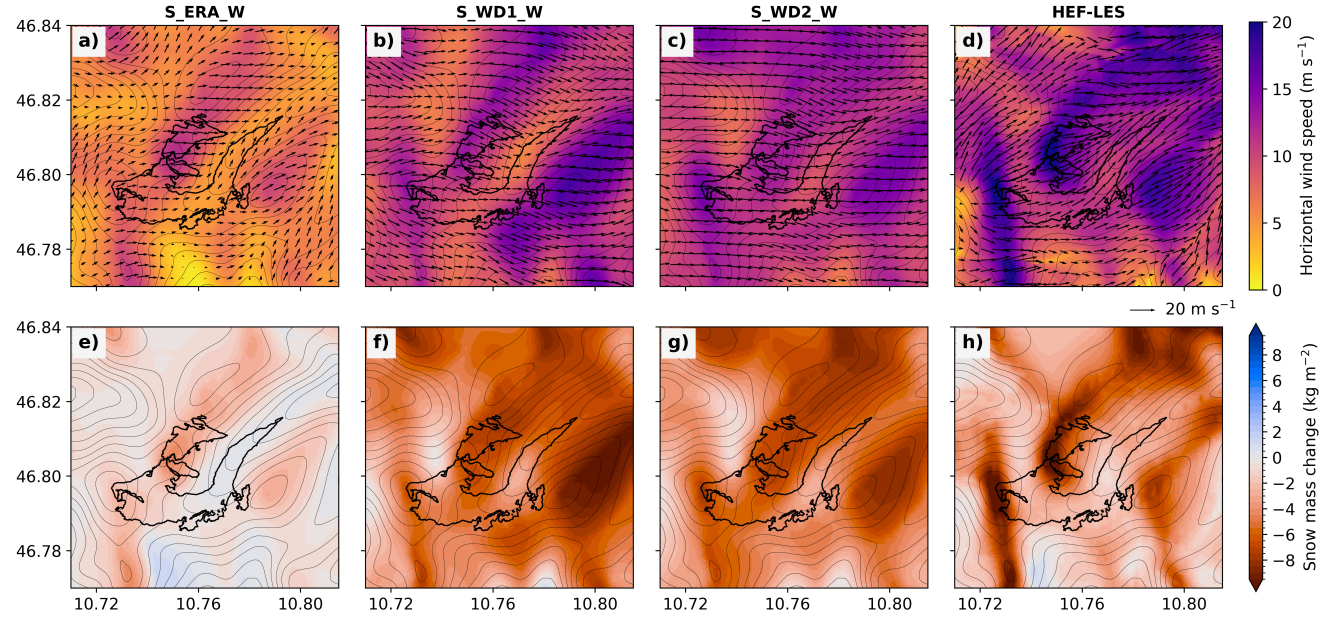

Figure 8. 10 m wind field (a–d) at 08 February 2021 21 UTC and snow mass change due to drifting snow accumulated over the entire day (e–h) for SNOWstorm driven with various input datasets and HEF-LES. Arrows in a–d depict the horizontal wind vector, model topography is shown by black contour lines with spacing of 100 m, outlines of Hintereisferner by thick black lines.

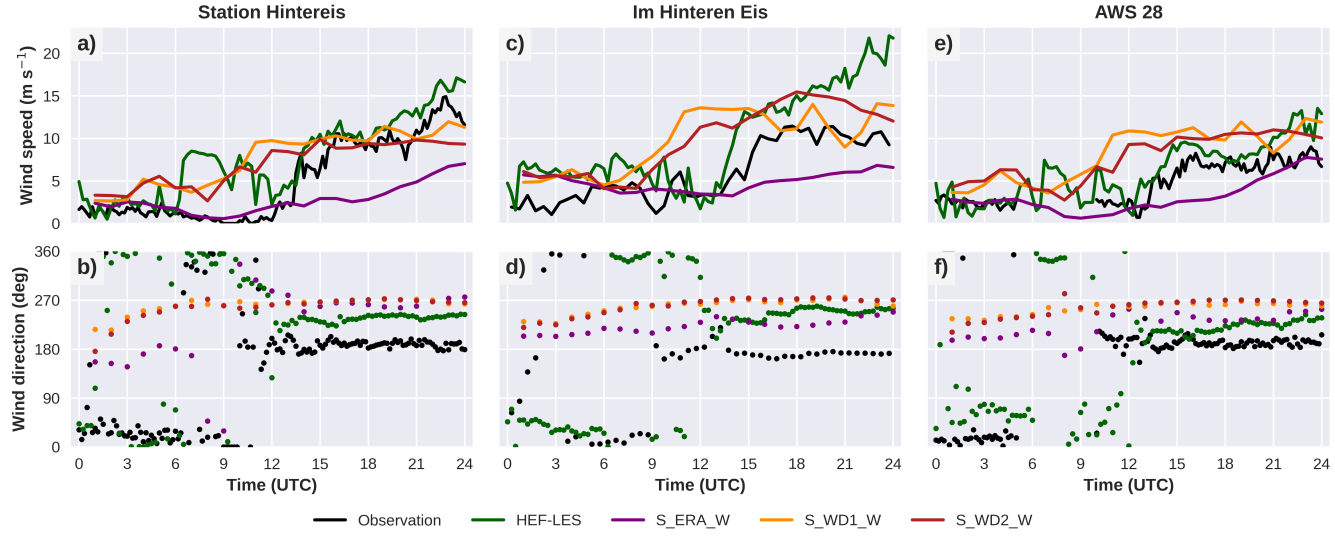

Figure 9. Time series for 08 February 2021 of wind speed and direction from observations at weather stations and model output of HEF-LES and SNOWstorm with input described in Tab. 2 at the corresponding closest grid point.

https://doi.org/10.5194/egusphere-2025-5608
Preprint. Discussion started: 16 January 2026

- Errors of SNOWstorm are comparable to other similar models with an MAE in near-surface wind speeds of about 0.8 $\mathrm{m\ s^{-1}}$ and bias of -0.12 $\mathrm{m\ s^{-1}}$. Errors slightly increase for situations with higher background wind speeds.

Key findings form the application case study are:

- SNOWstorm generally succeeds to capture the overall flow structure and redistribution patterns by the LES both with the smoothed topography from the LES and an un-smoothed high-resolution DEM.
- Wind velocities and flow features like deflection and acceleration around ridges are predicted well by SNOWstorm, however, the channeling effect inside the valleys is less pronounced leading to biases in wind direction in the ML-model.
- Validated against automatic weather stations, errors in the wind speed are slightly higher than in the crossvalidation experiments with MAEs between about 1.5 and 4 $\mathrm{m\ s^{-1}}$.
- Overall amounts of snow mass change as well as the placement of zones of erosion and deposition agree between SNOWstorm and the LES.
- Due to lack of information on the meso-scale flow structure, SNOWstorm driven with input from ERA5 predicts much lower wind speeds and redistribution amounts. Both experiments with meso-scale input ($\Delta x = 6$ km and $\Delta x = 1.2$ km) show similar results. This indicates that in this case all necessary information is already contained at the coarser 6 km resolution.
- One limitation of the model are localized effects of shallow cold-air advection and delayed local responses during transition phases in the large-scale forcing which not captured well by SNOWstorm as such effects have not been seen during training.

With the very large computational speedup of more than five orders of magnitude compared to physics-based LES at $\Delta x = 50$ m, the model has large potential to be used in (multi-) seasonal assessments of snow redistribution. For this, next steps will involve coupling SNOWstorm to glacier mass balance models like, e.g. COSIPY (Sauter et al., 2020) and extending the model for larger areas. Given the world-wide availability of high-resolution DEMs (e.g., European Space Agency, 2019) and the dependence on only a few standard atmospheric variables at meso-scale resolutions, recently published regional downscaling datasets in e.g. Europe (Copernicus Climate Change Service, 2022), the Alps (MeteoSwiss, 2025), South America (Dominguez et al., 2024), New Zealand (Kropač et al., 2024) or in arctic regions (Turton et al., 2020; Copernicus Climate Change Service, 2021) can provide possible input data sets for SNOWstorm applications. Apart from that, our results show the potential of generalization of emulator models trained under semi-idealized conditions given a carefully created training data set. Similar approaches could be possible e.g. for thermally driven flows or turbulent exchange of energy, mass and momentum in complex terrain.

Code and data availability. The current version of SNOWstorm is Saigger (2025), available at https://zenodo.org/records/17580745. The exact version of the model (v1.0) used to produce the results in this paper is archived on Zenodo under DOI 10.5281/zenodo.17580746.

https://doi.org/10.5194/egusphere-2025-5608
Preprint. Discussion started: 16 January 2026

The subset of the simulations used for the model training is available at Saigger (2025). The WRF snow drift module is available at Saigger (2024). Simulation output of the HEF-LES is available at Goger (2026). The output of the meso-scale WRF simulations used to drive the HEF-LES and SNOWstorm is available at Saigger et al. (2026). Meteorological data used in this study is available at ACINN (2025).

Author contributions. MS: conceptualization, development, training, application, and analysis of SNOWstorm, writing of original draft. BG: original HEF-LES simulations, interpretation of case study results, writing review and editing. TM: conceptualization, supervision, writing review and editing, funding acquisition.

Competing interests. The authors declare that they have no conflict of interest.

Acknowledgements. MS was funded by Elite Network of Bavaria—Bavarian State Ministy of Science and Art (Grand reference: IDP M3OCCA). BG was funded by the project "Measuring and modeling snow cover dynamics at high resolution for improving distributed mass balance research on mountain glaciers", a joint project fully funded by the Austrian Science Foundation (FWF; project number I 3841-N32) and the Deutsche Forschungsgemeinschaft (DFG; project number SA 2339/7-1). The authors gratefully acknowledge the scientific support and HPC resources provided by the Erlangen National High Performance Computing Center (NHR@FAU) of the Friedrich-Alexander-Universität Erlangen-Nürnberg (FAU) under the NHR project b128dc/ATMOS ("Numerical atmospheric modelling for the attribution of climate change and for model improvement"). NHR funding is provided by federal and Bavarian state authorities. NHR@FAU hardware is partially funded by the German Research Foundation (DFG)—440719683. We acknowledge financial support by Deutsche Forschungsgemeinschaft and Friedrich-Alexander-Universität Erlangen-Nürnberg within the funding programme "Open Access Publication Funding". We thank Christian Sommer for providing and helping with the GLO-30 data.

https://doi.org/10.5194/egusphere-2025-5608
Preprint. Discussion started: 16 January 2026

References

Abrahim, B. N., Cullen, N. J., Conway, J. P., and Sirguey, P.: Applying a distributed mass-balance model to identify uncertainties in glaciological mass balance on Brewster Glacier, New Zealand, J. Glaciol., pp. 1–17, https://doi.org/10.1017/jog.2022.123, 2023.

ACINN: ACINN Stations, Department of Atmospheric and Cryospheric Sciences, Universität Innsbruck, [data set], https://www.uibk.ac.at/projects/station-hintereis-opal-data/meteorology/, last access: 07 October 2025, 2025.

Amory, C., Gallée, H., Naaim-Bouvet, F., Favier, V., Vignon, E., Picard, G., Trouvilliez, A., Piard, L., Genthon, C., and Bellot, H.: Seasonal Variations in Drag Coefficient over a Sastrugi-Covered Snowfield in Coastal East Antarctica, Bound.-Lay. Meteorol., 164, 107–133, https://doi.org/10.1007/s10546-017-0242-5, 2017.

Blau, M. T., Turton, J. V., Sauter, T., and Mölg, T.: Surface mass balance and energy balance of the 79N Glacier (Nioghalvfjerdsfjorden, NE Greenland) modeled by linking COSIPY and Polar WRF, J. Glaciol., 67, 1093–1107, https://doi.org/10.1017/jog.2021.56, 2021.

Cooley, J. W. and Tukey, J. W.: An algorithm for the machine calculation of complex Fourier series, Math. Comp., 19, 297–301, https://doi.org/10.1090/S0025-5718-1965-0178586-1, 1965.

Copernicus Climate Change Service: Arctic regional reanalysis on pressure levels from 1991 to present, ECMWF, [data set], https://doi.org/10.24381/CDS.E3C841AD, 2021.

Copernicus Climate Change Service: CERRA sub-daily regional reanalysis data for Europe on pressure levels from 1984 to present, ECMWF, [data set], https://doi.org/10.24381/CDS.A39FF99F, 2022.

Cuffey, K. and Paterson, W. S. B.: The physics of glaciers, Butterworth-Heinemann/Elsevier, Burlington, MA, 4th edn., ISBN 978-0-12-369461-4, 2010.

Dadic, R., Mott, R., Lehning, M., and Burlando, P.: Wind influence on snow depth distribution and accumulation over glaciers, J. Geophys. Res., 115, F01 012, https://doi.org/10.1029/2009JF001261, 2010.

Deardorff, J. W.: Stratocumulus-capped mixed layers derived from a three-dimensional model, Bound.-Lay. Meteor., 18, 495–527, https://doi.org/10.1007/BF00119502, 1980.

Dominguez, F., Rasmussen, R., Liu, C., Ikeda, K., Prein, A., Varble, A., Arias, P. A., Bacmeister, J., Bettolli, M. L., Callaghan, P., Carvalho, L. M. V., Castro, C. L., Chen, F., Chug, D., Chun, K. P. S., Dai, A., Danaila, L., da Rocha, R. P., Nascimento, E. d. L., Dougherty, E., Dudhia, J., Eidhammer, T., Feng, Z., Fita, L., Fu, R., Giles, J., Gilmour, H., Halladay, K., Huang, Y., Iza Wong, A. M., Lagos-Zúñiga, M. A., Jones, C., Llamocca, J., Llopart, M., Martinez, J. A., Martinez, J. C., Minder, J. R., Morrison, M., Moon, Z. L., Mu, Y., Neale, R. B., Núñez Ocasio, K. M., Pal, S., Potter, E., Poveda, G., Puhales, F., Rasmussen, K. L., Rehbein, A., Rios-Berrios, R., Risanto, C. B., Rosales, A., Scaff, L., Seimon, A., Somos-Valenzuela, M., Tian, Y., Van Oevelen, P., Veloso-Aguila, D., Xue, L., and Schneider, T.: Advancing South American Water and Climate Science through Multidecadal Convection-Permitting Modeling, Bull. Amer. Meteor. Soc., 105, E32–E44, https://doi.org/10.1175/BAMS-D-22-0226.1, 2024.

Dujardin, J. and Lehning, M.: Wind-Topo: Downscaling near-surface wind fields to high-resolution topography in highly complex terrain with deep learning, Q. J. R. Meteor. Soc., 148, 1368–1388, https://doi.org/10.1002/qj.4265, 2022.

Dupuy, F., Durand, P., and Hedde, T.: Downscaling of surface wind forecasts using convolutional neural networks, Nonlin. Processes Geophys., 30, 553–570, https://doi.org/10.5194/npg-30-553-2023, 2023.

Déry, S. J. and Yau, M. K.: A Bulk Blowing Snow Model, Bound.-Lay. Meteorol., 93, 237–251, https://doi.org/10.1023/A:1002065615856, 1999.

https://doi.org/10.5194/egusphere-2025-5608
Preprint. Discussion started: 16 January 2026

European Space Agency: Copernicus DEM - Global and European Digital Elevation Model, ESA, [data set], https://doi.org/https://doi.org/10.5270/ESA-c5d3d65, 2019.

Filhol, S. and Sturm, M.: Snow bedforms: A review, new data, and a formation model: Snow bedforms: Review and Modeling, J. Geophys. Res. Earth Surf., 120, 1645–1669, https://doi.org/10.1002/2015JF003529, 2015.

Fitzpatrick, N., Radić, V., and Menounos, B.: A multi-season investigation of glacier surface roughness lengths through in situ and remote observation, The Cryosphere, 13, 1051–1071, https://doi.org/10.5194/tc-13-1051-2019, 2019.

Gascoin, S., Lhermitte, S., Kinnard, C., Bortels, K., and Liston, G. E.: Wind effects on snow cover in Pascua-Lama, Dry Andes of Chile, Adv. Water Resour., 55, 25–39, https://doi.org/10.1016/j.advwatres.2012.11.013, 2013.

Gerber, F., Besic, N., Sharma, V., Mott, R., Daniels, M., Gabella, M., Berne, A., Germann, U., and Lehning, M.: Spatial variability in snow precipitation and accumulation in COSMO–WRF simulations and radar estimations over complex terrain, The Cryosphere, 12, 3137–3160, https://doi.org/10.5194/tc-12-3137-2018, 2018.

Gerber, F., Mott, R., and Lehning, M.: The Importance of Near-Surface Winter Precipitation Processes in Complex Alpine Terrain, J. Hydrometeor., 20, 177–196, https://doi.org/10.1175/JHM-D-18-0055.1, 2019.

Goger, B.: HEF-LES simulations, https://doi.org/10.5281/zenodo.18206320, 2026.

Goger, B., Stiperski, I., Nicholson, L., and Sauter, T.: Large-eddy simulations of the atmospheric boundary layer over an Alpine glacier: Impact of synoptic flow direction and governing processes, Q. J. R. Meteor. Soc., 148, 1319–1343, https://doi.org/10.1002/qj.4263, 2022.

Goodfellow, I., Bengio, Y., and Courville, A.: Deep Learning, MIT Press, http://www.deeplearningbook.org, 2016.

Groot Zwaaftink, C. D., Löwe, H., Mott, R., Bavay, M., and Lehning, M.: Drifting snow sublimation: A high-resolution 3-D model with temperature and moisture feedbacks, J. Geophys. Res., 116, D16 107, https://doi.org/10.1029/2011JD015754, 2011.

Gutmann, E., Barstad, I., Clark, M., Arnold, J., and Rasmussen, R.: The Intermediate Complexity Atmospheric Research Model (ICAR), J. Hydrometeor., 17, 957–973, https://doi.org/10.1175/JHM-D-15-0155.1, 2016.

Göbel, M., Serafin, S., and Rotach, M. W.: Numerically consistent budgets of potential temperature, momentum, and moisture in Cartesian coordinates: application to the WRF model, Geosci. Model Dev., 15, 669–681, https://doi.org/10.5194/gmd-15-669-2022, 2022.

Helbig, N. and Löwe, H.: Shortwave radiation parameterization scheme for subgrid topography, J. Geophys. Res., 117, https://doi.org/10.1029/2011JD016465, 2012.

Helbig, N., Mott, R., van Herwijnen, A., Winstral, A., and Jonas, T.: Parameterizing surface wind speed over complex topography, J. Geophys. Res.: Atmos., 122, 651–667, https://doi.org/10.1002/2016JD025593, 2017.

Helbig, N., Mott, R., Bühler, Y., Le Toumelin, L., and Lehning, M.: Snowfall deposition in mountainous terrain: a statistical downscaling scheme from high-resolution model data on simulated topographies, Front. Earth Sci., 11, 1308 269, https://doi.org/10.3389/feart.2023.1308269, 2024.

Horak, J., Hofer, M., Gutmann, E., Gohm, A., and Rotach, M. W.: A process-based evaluation of the Intermediate Complexity Atmospheric Research Model (ICAR) 1.0.1, Geosci. Model Dev., 14, 1657–1680, https://doi.org/10.5194/gmd-14-1657-2021, 2021.

Houze, R. A.: Orographic effects on precipitating clouds, Rev. Geophys., 50, RG1001, https://doi.org/10.1029/2011RG000365, 2012.

Höhlein, K., Kern, M., Hewson, T., and Westermann, R.: A comparative study of convolutional neural network models for wind field downscaling, Meteorol. Appl., 27, https://doi.org/10.1002/met.1961, 2020.

Jacobs, T. D. B., Junge, T., and Pastewka, L.: Quantitative characterization of surface topography using spectral analysis, Surf. Topogr.: Metrol. Prop., 5, 013 001, https://doi.org/10.1088/2051-672X/aa51f8, 2017.

https://doi.org/10.5194/egusphere-2025-5608
Preprint. Discussion started: 16 January 2026

Jiménez, P. A. and Dudhia, J.: Improving the Representation of Resolved and Unresolved Topographic Effects on Surface Wind in the WRF Model, J. Appl. Meteor. Climatol., 51, 300–316, https://doi.org/10.1175/JAMC-D-11-084.1, 2012.

Khadka, A., Brun, F., Wagnon, P., Shrestha, D., and Sherpa, T. C.: Surface energy and mass balance of Mera Glacier (Nepal, Central Himalaya) and their sensitivity to temperature and precipitation, J. Glaciol., 70, e80, https://doi.org/10.1017/jog.2024.42, 2024.

Kirshbaum, D. J. and Durran, D. R.: Factors Governing Cellular Convection in Orographic Precipitation, J. Atmos. Sci., 61, 682–698, https://doi.org/10.1175/1520-0469(2004)061<0682:FGCCIO>2.0.CO;2, 2004.

Krieger, N., Wernli, H., Sprenger, M., and Kühnlein, C.: Revealing the dynamics of a local Alpine windstorm using large-eddy simulations, Wea. Clim. Dynam., 6, 447–469, https://doi.org/10.5194/wcd-6-447-2025, 2025.

Kropač, E., Mölg, T., and Cullen, N. J.: A new, high-resolution atmospheric dataset for southern New Zealand, 2005–2020, Geosci. Data J., p. gdj3.263, https://doi.org/10.1002/gdj3.263, 2024.

Lambrecht, A. and Mayer, C.: The role of the cryosphere for runoff in a highly glacierised alpine catchment, an approach with a coupled model and in situ data, J. Glaciol., pp. 1–14, https://doi.org/10.1017/jog.2024.48, 2024.

Le Toumelin, L., Gouttevin, I., Helbig, N., Galiez, C., Roux, M., and Karbou, F.: Emulating the Adaptation of Wind Fields to Complex Terrain with Deep Learning, Artif. Intell. Earth Syst., 2, e220 034, https://doi.org/10.1175/AIES-D-22-0034.1, 2023.

LeCun, Y., Bengio, Y., and Hinton, G.: Deep learning, Nature, 521, 436–444, https://doi.org/10.1038/nature14539, 2015.

Liston, G. E. and Elder, K.: A Meteorological Distribution System for High-Resolution Terrestrial Modeling (MicroMet), J. Hydrometeor., 7, 217–234, https://doi.org/10.1175/JHM486.1, 2006.

Liston, G. E. and Sturm, M.: A snow-transport model for complex terrain, J. Glaciol., 44, 498–516, https://doi.org/10.3189/S0022143000002021, 1998.

Lundquist, J. D., Vano, J., Gutmann, E., Hogan, D., Schwat, E., Haugeneder, M., Mateo, E., Oncley, S., Roden, C., Osenga, E., and Carver, L.: Sublimation of Snow, Bull. Amer. Meteor. Soc., 105, E975–E990, https://doi.org/10.1175/BAMS-D-23-0191.1, 2024.

Marsh, C. B., Vionnet, V., and Pomeroy, J. W.: Windmapper: An Efficient Wind Downscaling Method for Hydrological Models, Water Resour. Res., 59, e2022WR032 683, https://doi.org/10.1029/2022WR032683, 2023.

MeteoSwiss: ICON Reanalysis-Light-CH1 Dataset for the Alpine region [data set], https://doi.org/10.18751/NWP/REA-L-CH1/1.0, 2025.

Miralles, O., Steinfeld, D., Martius, O., and Davison, A. C.: Downscaling of Historical Wind Fields over Switzerland Using Generative Adversarial Networks, Artif. Intell. Earth Syst., 1, e220 018, https://doi.org/10.1175/AIES-D-22-0018.1, 2022.

Molina, M. J., O'Brien, T. A., Anderson, G., Ashfaq, M., Bennett, K. E., Collins, W. D., Dagon, K., Restrepo, J. M., and Ullrich, P. A.: A Review of Recent and Emerging Machine Learning Applications for Climate Variability and Weather Phenomena, Artif. Intell. Earth Syst., 2, 220 086, https://doi.org/10.1175/AIES-D-22-0086.1, 2023.

Mortezapour, M., Menounos, B., Jackson, P. L., Erler, A. R., and Pelto, B. M.: The role of meteorological forcing and snow model complexity in winter glacier mass balance estimation, Columbia River basin, Canada, Hydrol. Processes, 34, 5085–5103, https://doi.org/10.1002/hyp.13929, 2020.

Mott, R. and Lehning, M.: Meteorological Modeling of Very High-Resolution Wind Fields and Snow Deposition for Mountains, J. Hydrometeor., 11, 934–949, https://doi.org/10.1175/2010JHM1216.1, 2010.

Mott, R., Schirmer, M., Bavay, M., Grünewald, T., and Lehning, M.: Understanding snow-transport processes shaping the mountain snow-cover, The Cryosphere, 4, 545–559, https://doi.org/10.5194/tc-4-545-2010, 2010.

Mott, R., Schirmer, M., and Lehning, M.: Scaling properties of wind and snow depth distribution in an Alpine catchment, J. Geophys. Res., 116, D06 106, https://doi.org/10.1029/2010JD014886, 2011.

https://doi.org/10.5194/egusphere-2025-5608
Preprint. Discussion started: 16 January 2026

Mott, R., Scipión, D., Schneebeli, M., Dawes, N., Berne, A., and Lehning, M.: Orographic effects on snow deposition patterns in mountainous terrain, J. Geophys. Res.: Atmos., 119, 1419–1439, https://doi.org/10.1002/2013JD019880, 2014.

Mott, R., Vionnet, V., and Grünewald, T.: The Seasonal Snow Cover Dynamics: Review on Wind-Driven Coupling Processes, Front. Earth Sci., 6, 197, https://doi.org/10.3389/feart.2018.00197, 2018.

Nakanishi, M. and Niino, H.: An Improved Mellor–Yamada Level-3 Model: Its Numerical Stability and Application to a Regional Prediction of Advection Fog, Bound.-Lay. Meteor., 119, 397–407, https://doi.org/10.1007/s10546-005-9030-8, 2006.

Noël, B., Lhermitte, S., Wouters, B., and Fettweis, X.: Poleward shift of subtropical highs drives Patagonian glacier mass loss, Nat. Commun., 16, 3795, https://doi.org/10.1038/s41467-025-58974-1, 2025.

Oulkar, S. N., Sharma, P., Pratap, B., Thamban, M., Laha, S., Patel, L. K., and Singh, A. T.: Distributed energy balance, mass balance and climate sensitivity of upper Chandra Basin glaciers, western Himalaya, Ann. Glaciol., 66, e5, https://doi.org/10.1017/aog.2024.46, 2025.

Reynolds, D., Gutmann, E., Kruyt, B., Haugeneder, M., Jonas, T., Gerber, F., Lehning, M., and Mott, R.: The High-resolution Intermediate Complexity Atmospheric Research (HICAR v1.1) model enables fast dynamic downscaling to the hectometer scale, Geosci. Model Dev., 16, 5049–5068, https://doi.org/10.5194/gmd-16-5049-2023, 2023.

Reynolds, D., Quéno, L., Lehning, M., Jafari, M., Berg, J., Jonas, T., Haugeneder, M., and Mott, R.: Seasonal snow–atmosphere modeling: let's do it, The Cryosphere, 18, 4315–4333, https://doi.org/10.5194/tc-18-4315-2024, 2024.

Ronneberger, O., Fischer, P., and Brox, T.: U-Net: Convolutional Networks for Biomedical Image Segmentation, in: Medical Image Computing and Computer-Assisted Intervention – MICCAI 2015, edited by Navab, N., Hornegger, J., Wells, W. M., and Frangi, A. F., vol. 9351, pp. 234–241, Springer International Publishing, Cham, ISBN 978-3-319-24573-7 978-3-319-24574-4, https://doi.org/10.1007/978-3-319-24574-4_28, series Title: Lecture Notes in Computer Science, 2015.

Saigger, M.: WRFsnowdrift, Zenodo, [code], https://doi.org/10.5281/zenodo.10837359, 2024.

Saigger, M.: SNOWstorm v1.0, Zenodo, [code], https://doi.org/10.5281/zenodo.17580746, 2025.

Saigger, M., Sauter, T., Schmid, C., Collier, E., Goger, B., Kaser, G., Prinz, R., Voordendag, A., and Mölg, T.: A Drifting and Blowing Snow Scheme in the Weather Research and Forecasting Model, J. Adv. Model Earth Syst., 16, e2023MS004007, https://doi.org/10.1029/2023MS004007, 2024.

Saigger, M., Goger, B., and Mölg, T.: Model output for "SNOWstorm (v1.0) - a deep- learning based model for near-surface winds and drifting snow in mountain environments", https://doi.org/10.5281/zenodo.18184973, 2026.

Salvador, R., Calbó, J., and Millán, M. M.: Horizontal Grid Size Selection and its Influence on Mesoscale Model Simulations, J. Appl. Meteor., 38, 1311–1329, https://doi.org/10.1175/1520-0450(1999)038<1311:HGSSAI>2.0.CO;2, 1999.

Sauter, T.: Revisiting extreme precipitation amounts over southern South America and implications for the Patagonian Icefields, Hydrol. Earth Syst. Sci., 24, 2003–2016, https://doi.org/10.5194/hess-24-2003-2020, 2020.

Sauter, T., Möller, M., Finkelnburg, R., Grabiec, M., Scherer, D., and Schneider, C.: Snowdrift modelling for the Vestfonna ice cap, north-eastern Svalbard, The Cryosphere, 7, 1287–1301, https://doi.org/10.5194/tc-7-1287-2013, 2013.

Sauter, T., Arndt, A., and Schneider, C.: COSIPY v1.3 – an open-source coupled snowpack and ice surface energy and mass balance model, Geosci. Model Dev., 13, 5645–5662, https://doi.org/10.5194/gmd-13-5645-2020, 2020.

Sauter, T., Brock, B. W., Collier, E., Georgi, A., Goger, B., Groos, A. R., Haualand, K. F., Haugeneder, M., Mandal, A., Mott, R., Nicholson, L., Prinz, R., Reynolds, D., Saigger, M., Shaw, T. E., Sicart, J. E., Stiperski, I., and Voordendag, A.: Glacier-Atmosphere Interactions and Feedbacks in High-Mountain Regions - A Review, https://doi.org/10.22541/essoar.174164160.03475851/v1, 2025.

https://doi.org/10.5194/egusphere-2025-5608
Preprint. Discussion started: 16 January 2026

Schirmer, M., Wirz, V., Clifton, A., and Lehning, M.: Persistence in intra-annual snow depth distribution: 1. Measurements and topographic control, Water Resour. Res., 47, https://doi.org/10.1029/2010WR009426, 2011.

Sekiyama, T. T., Hayashi, S., Kaneko, R., and Fukui, K.-i.: Surrogate Downscaling of Mesoscale Wind Fields Using Ensemble Superresolution Convolutional Neural Networks, Artif. Intell. Earth Syst., 2, 230 007, https://doi.org/10.1175/AIES-D-23-0007.1, 2023.

Sharma, V., Gerber, F., and Lehning, M.: Introducing CRYOWRF v1.0: multiscale atmospheric flow simulations with advanced snow cover modelling, Geosci. Model Dev., 16, 719–749, https://doi.org/10.5194/gmd-16-719-2023, 2023.

Sigmund, A., Melo, D. B., Dujardin, J., Nishimura, K., and Lehning, M.: Parameterizing Snow Sublimation in Conditions of Drifting and Blowing Snow, J. Adv. Model Earth Syst., 17, e2024MS004 332, https://doi.org/10.1029/2024MS004332, 2025.

Skamarock, W. C., Klemp, J. B., Dudhia, J., Gill, D. O., Liu, Z., Berner, J., Wang, W., Powers, J. G., Duda, M. G., Barker, D. M., and Huang, X.-Y.: A Description of the Advanced Research WRF Model Version 4, Tech. rep., UCAR/NCAR, https://doi.org/10.5065/1DFH-6P97, 2019.

Smith, R. B. and Barstad, I.: A Linear Theory of Orographic Precipitation, J. Atmos. Sci., 61, 1377–1391, https://doi.org/10.1175/1520-0469(2004)061<1377:ALTOOP>2.0.CO;2, 2004.

Steyn, D. G. and Ayotte, K. W.: Application of Two-Dimensional Terrain Height Spectra to Mesoscale Modeling, J. Atmos. Sci., 42, 2884–2887, https://doi.org/10.1175/1520-0469(1985)042<2884:aotdth>2.0.co;2, 1985.

Strasser, U., Bernhardt, M., Weber, M., Liston, G. E., and Mauser, W.: Is snow sublimation important in the alpine water balance?, The Cryosphere, 2, 53–66, https://doi.org/10.5194/tc-2-53-2008, 2008.

Temme, F., Farías-Barahona, D., Seehaus, T., Jaña, R., Arigony-Neto, J., Gonzalez, I., Arndt, A., Sauter, T., Schneider, C., and Fürst, J. J.: Strategies for regional modeling of surface mass balance at the Monte Sarmiento Massif, Tierra del Fuego, The Cryosphere, 17, 2343–2365, https://doi.org/10.5194/tc-17-2343-2023, 2023.

Temme, F., Sommer, C., Schaefer, M., Jaña, R., Arigony-Neto, J., Gonzalez, I., Izagirre, E., Giesecke, R., Tetzner, D., and Fürst, J. J.: Climate's firm grip on glacier ablation in the Cordillera Darwin Icefield, Tierra del Fuego, Nat. Commun., 16, 2677, https://doi.org/10.1038/s41467-025-57698-6, 2025.

Terleth, Y., van Pelt, W. J. J., and Pettersson, R.: Spatial variability in winter mass balance on Storglaciären modelled with a terrain-based approach, J. Glaciol., 69, 749–761, https://doi.org/10.1017/jog.2022.96, 2023.

Turton, J. V., Mölg, T., and Collier, E.: High-resolution (1 km) Polar WRF output for 79° N Glacier and the northeast of Greenland from 2014 to 2018, Earth Syst. Sci. Data, 12, 1191–1202, https://doi.org/10.5194/essd-12-1191-2020, 2020.

Umek, L., Gohm, A., Haid, M., Ward, H. C., and Rotach, M. W.: Large-eddy simulation of foehn–cold pool interactions in the Inn Valley during PIANO IOP 2, Q. J. R. Meteorol. Soc., 147, 944–982, https://doi.org/10.1002/qj.3954, 2021.

van der Meer, M., de Roda Husman, S., and Lhermitte, S.: Deep Learning Regional Climate Model Emulators: A Comparison of Two Downscaling Training Frameworks, J. Adv. Model Earth Syst., 15, e2022MS003 593, https://doi.org/10.1029/2022MS003593, 2023.

Vionnet, V., Guyomarc'h, G., Naaim Bouvet, F., Martin, E., Durand, Y., Bellot, H., Bel, C., and Puglièse, P.: Occurrence of blowing snow events at an alpine site over a 10-year period: Observations and modelling, Adv. Water Resour., 55, 53–63, https://doi.org/10.1016/j.advwatres.2012.05.004, 2013.

Vionnet, V., Martin, E., Masson, V., Guyomarc'h, G., Naaim-Bouvet, F., Prokop, A., Durand, Y., and Lac, C.: Simulation of wind-induced snow transport and sublimation in alpine terrain using a fully coupled snowpack/atmosphere model, The Cryosphere, 8, 395–415, https://doi.org/10.5194/tc-8-395-2014, 2014.

https://doi.org/10.5194/egusphere-2025-5608
Preprint. Discussion started: 16 January 2026

Vionnet, V., Martin, E., Masson, V., Lac, C., Naaim Bouvet, F., and Guyomarc'h, G.: High-Resolution Large Eddy Simulation of Snow Accumulation in Alpine Terrain, J. Geophys. Res.: Atmos., 122, 11,005–11,021, https://doi.org/10.1002/2017JD026947, 2017.

Vionnet, V., Marsh, C. B., Menounos, B., Gascoin, S., Wayand, N. E., Shea, J., Mukherjee, K., and Pomeroy, J. W.: Multi-scale snowdrift-permitting modelling of mountain snowpack, The Cryosphere, 15, 743–769, https://doi.org/10.5194/tc-15-743-2021, 2021.

Voordendag, A., Goger, B., Prinz, R., Sauter, T., Mölg, T., Saigger, M., and Kaser, G.: A novel framework to investigate wind-driven snow redistribution over an Alpine glacier: combination of high-resolution terrestrial laser scans and large-eddy simulations, The Cryosphere, 18, 849–868, https://doi.org/10.5194/tc-18-849-2024, 2024.

Wagenbrenner, N. S., Forthofer, J. M., Lamb, B. K., Shannon, K. S., and Butler, B. W.: Downscaling surface wind predictions from numerical weather prediction models in complex terrain with WindNinja, Atmos. Chem. Phys., 16, 5229–5241, https://doi.org/10.5194/acp-16-5229-2016, 2016.

Warscher, M., Strasser, U., Kraller, G., Marke, T., Franz, H., and Kunstmann, H.: Performance of complex snow cover descriptions in a distributed hydrological model system: A case study for the high Alpine terrain of the Berchtesgaden Alps, Water Resour. Res., 49, 2619–2637, https://doi.org/10.1002/wrcr.20219, 2013.

Weiss, A.: Topographic position and landform analysis, http://www.jennessent.com/downloads/tpi-poster-tnc_18x22.pdf, 2001.

Winstral, A. and Marks, D.: Simulating wind fields and snow redistribution using terrain-based parameters to model snow accumulation and melt over a semi-arid mountain catchment, Hydrol. Processes, 16, 3585–3603, https://doi.org/10.1002/hyp.1238, 2002.

Winstral, A., Elder, K., and Davis, R. E.: Spatial Snow Modeling of Wind-Redistributed Snow Using Terrain-Based Parameters, J. Hydrometeor, 3, 524–538, https://doi.org/10.1175/1525-7541(2002)003<0524:SSMOWR>2.0.CO;2, 2002.

Young, G. S. and Pielke, R. A.: Application of Terrain Height Variance Spectra to Mesoscale Modeling, J. Atmos. Sci., 40, 2555–2560, https://doi.org/10.1175/1520-0469(1983)040<2555:AOTHVS>2.0.CO;2, 1983.

Zhang, X., Bao, J.-W., Chen, B., and Grell, E. D.: A Three-Dimensional Scale-Adaptive Turbulent Kinetic Energy Scheme in the WRF-ARW Model, Mon. Wea. Rev., 146, 2023–2045, https://doi.org/10.1175/MWR-D-17-0356.1, 2018.

Zängl, G.: Interaction between Dynamics and Cloud Microphysics in Orographic Precipitation Enhancement: A High-Resolution Modeling Study of Two North Alpine Heavy-Precipitation Events, Mon. Wea. Rev., 135, 2817–2840, https://doi.org/10.1175/MWR3445.1, 2007.